

The Formation and Evolution of Planetary Systems: Placing Our Solar System in Context with Spitzer

Michael R. Meyer

Steward Observatory, The University of Arizona

`mmeyer@as.arizona.edu`

Lynne A. Hillenbrand

California Institute of Technology

Dana Backman

SOFIA/SETI Institute

Steve Beckwith

Space Telescope Science Institute

Department of Physics and Astronomy, Johns Hopkins University

Jeroen Bouwman

Max-Planck-Institut für Astronomie, Heidelberg

Tim Brooke

California Institute of Technology

John Carpenter

California Institute of Technology

Martin Cohen

Radio Astronomy Laboratory, University of California–Berkeley

Stephanie Cortes

Steward Observatory, The University of Arizona

Nathan Crockett

National Optical Astronomy Observatories

Uma Gorti

NASA-Ames Research Center, Theory Branch

Thomas Henning

Max-Planck-Institut für Astronomie, Heidelberg

Dean Hines

Space Science Institute

David Hollenbach

NASA-Ames Research Center, Theory Branch

Jinyoung Serena Kim

Steward Observatory, The University of Arizona

Jonathan Lunine

Lunar and Planetary Laboratory, The University of Arizona

Renu Malhotra

Lunar and Planetary Laboratory, The University of Arizona

Eric Mamajek

Harvard-Smithsonian Center for Astrophysics

Stanimir Metchev

The University of California, Los Angeles

Amaya Moro-Martin

Department of Astrophysical Science, Princeton University

Pat Morris

Herschel Science Center, IPAC

Joan Najita

National Optical Astronomy Observatories

Deborah Padgett

Spitzer Science Center

Ilaria Pascucci

Steward Observatory, The University of Arizona

Jens Rodmann

Max-Planck-Institut für Astronomie, Heidelberg

Wayne Schlingman

Steward Observatory, The University of Arizona

Murray Silverstone

Steward Observatory, The University of Arizona

David Soderblom

Space Telescope Science Institute

John Stauffer

Spitzer Science Center

Elizabeth Stobie

Steward Observatory, The University of Arizona

Steve Strom

National Optical Astronomy Observatories

Dan Watson

Department of Physics and Astronomy, The University of Rochester

Stuart Weidenschilling

Planetary Science Institute

Sebastian Wolf

Max-Planck-Institut für Astronomie, Heidelberg

Erick Young

Steward Observatory, The University of Arizona

ABSTRACT

We provide an overview of the Spitzer Legacy Program “Formation and Evolution of Planetary Systems” (FEPS) which was proposed in 2000, begun in 2001, and executed aboard the Spitzer Space Telescope between 2003 and 2006. This program exploits the sensitivity of Spitzer to carry out mid-infrared spectrophotometric observations of solar-type stars. With a sample of ~ 328 stars ranging in age from ~ 3 Myr to ~ 3 Gyr, we trace the evolution of circumstellar gas and dust from primordial planet-building stages in young circumstellar disks through to older collisionally generated debris disks. When completed, our program will help define the time scales over which terrestrial and gas giant planets are built, constrain the frequency of planetesimal collisions as a function of time, and establish the diversity of mature planetary architectures.

In addition to the observational program, we have coordinated a concomitant theoretical effort aimed at understanding the dynamics of circumstellar dust with and without the effects of embedded planets, dust spectral energy distributions, and atomic and molecular gas line emission. Together with the observations, these efforts will provide astronomical context for understanding whether our Solar System – and its habitable planet – is a common or a rare circumstance. Additional information about the FEPS project can be found on the team website:

<http://feeps.as.arizona.edu/>

Subject headings: infrared: general, space vehicles: Spitzer Space Telescope, surveys, stars: circumstellar matter

1. Introduction

The Spitzer Space Telescope (Werner et al. 2004), formerly SIRTf the **S**pace **I**nfra**R**ed **T**elescope **F**acility, is an 85 cm cryogenic space observatory in earth-trailing orbit. The observatory was launched in August of 2003 and has an estimated mission lifetime of 5+ years. There are three science instruments on-board: IRAC (Fazio et al. 2004), IRS (Houck et al. 2004), and MIPS (Rieke et al. 2004) which together provide the capability for imaging and spectroscopy from 3.6–160 μ m. The Legacy Science Program was established before launch with two goals: to enable large scale programs of broad scientific and public interest, and to provide access to uniform and coherent datasets as rapidly as possible in support of General Observer (GO) proposals, given the limited lifetime of the mission. The Formation and Evolution of Planetary Systems (FEPS) Spitzer Legacy Science Program is one of six such original programs (for descriptions of the others see Evans et al. 2003; Benjamin et al. 2003; Kenicutt et al. 2003; Lonsdale et al. 2003; Dickenson et al. 2003) and uses 350 hours of Spitzer observing time. FEPS builds upon the rich heritage of Spitzer’s ancestors in space: the international all-sky mid-infrared survey telescope IRAS (the Infrared Astronomical Satellite, 1983–1985) and ESA’s pointed mission ISO (the Infrared Space Observatory, 1995–1999), and complements Guaranteed Time Observer (GTO) and GO programs also being pursued with Spitzer.

In a single sentence, FEPS is a comprehensive study of the evolution of gas and dust in the circumstellar environment. The scientific motivation for FEPS lies in the fragmented but compelling evidence for dusty circumstellar material surrounding stars spanning a wide range of ages, from young pre-main sequence stars to those as old as, and even older than, the Sun.

At young ages, incontrovertible evidence assembled over the past three decades (based on data from ultraviolet through millimeter wavelengths), suggests that most stars are surrounded at birth by accretion disks that are remnants of the star formation process itself (e.g. Beckwith and Sargent, 1996). The revelations provided by IRAS, and later ISO, led to a nearly complete census of optically-thick disks within 100-200 pc, and in the case of ISO revealed their rich dust mineralogy and gas content (see Lorenzetti 2005 and Molster & Kemper 2005 for reviews). That at least some of these disks build planets has become clear from radial velocity and photometric studies revealing $M \sin i = 0.02\text{--}15 M_J$ planets orbiting well over one hundred nearby stars (e.g. Marcy et al. 2005). At older ages, IRAS and ISO revealed the presence around dozens of main sequence stars of micron-sized grains. These dusty “debris” disks are produced in collisions between asteroid-like bodies with orbits that are dynamically stirred by planets (e.g. Lagrange et al. 2000). Subsequently, several of these disks were spatially resolved at optical, infrared, and millimeter wavelengths (e.g. Kalas, Liu, & Mathews 2004; Weinberger et al. 1999; Greaves et al. 1998) revealing structure consistent with the planetary perturber interpretation.

The connections between planets, debris disks, and the dusty and gaseous disks near-ubiquitously found in association with recently formed young stars are tantalizing, but not yet unequivocally established. Understanding the evolution of young circumstellar dust and gas disks as they transition through the planet-building phase requires the hundred-fold enhancement in sensitivity and increased photometric accuracy offered by Spitzer at mid- and far-infrared wavelengths. For main sequence stars, while IRAS discovered the prototypical debris disks (see Backman & Paresce 1993 for a review) and ISO made additional surveys (see de Muizon 2005 for a review), neither IRAS nor ISO was sensitive enough to detect dust in solar systems older than a few hundred Myr for any but the nearest tens of stars ¹. Spitzer, by contrast can detect orders of magnitude smaller dust masses: for a solar-type star at 30 pc, down to $\sim 10^{20}$ kg or $\sim 10^{-5} M_{Earth}$ in

¹The IRAS and ISO observatories were able to study representative samples of A-type stars, but not G-type stars.

micron to sub-millimeter size grains at 50 K, only an order of magnitude above the dust mass inferred for our own present-day Kuiper Belt, and $\sim 10^{17}$ kg or $\sim 10^{-8} M_{Earth}$ at 150 K, only an order of magnitude above the dust mass in our present-day asteroid belt plus zodiacal cloud.

The FEPS program is designed to study circumstellar dust properties around a representative sample of solar-type stars. Included are 328 stars chosen to probe the suspected direct link between disks commonly found around pre-main sequence stars < 3.0 Myr old and our 4.56 Gyr old Sun and Solar System. Specifically, we trace the evolution of circumstellar material at ages 3-10 Myr when stellar accretion from the disk terminates, to 10-100 Myr when planets achieve their final masses via coalescence of solids and accretion of remnant molecular gas, to 100-1000 Myr when the final architecture of solar systems takes form and frequent collisions between remnant planetesimals produce copious quantities of dust, and finally, to 1-3 Gyr mature systems in which planet-driven activity of planetesimals continues to generate detectable dust. Our sample is distributed uniformly in log-age from 3 Myr to 3 Gyr. We probe the full range of dust disk optical-depths diagnostic of the major phases of planet system formation and evolution, including primordial disks (those dominated by ISM grains in the process of agglomerating into planetesimals) and debris disks (those dominated by collisionally generated dust) like our own.

Our strategy is to obtain for all 328 stars in our sample carefully calibrated spectral energy distributions (SEDs) using all three Spitzer instruments. A high-resolution spectroscopic survey limited to the younger targets establishes the gas content. In addition to insight into problems of fundamental scientific and philosophical interest, the FEPS Legacy Science Program provides a rich database for follow-up observations with Spitzer, with existing and future ground-based facilities, as well as SIM and JWST, and eventually TPF. FEPS complements and motivates many existing Spitzer GTO and GO programs.

2. Science Strategy

We take advantage of Spitzer’s unprecedented mid-infrared sensitivity and hence its unique ability to detect the photospheres of solar-type stars out to distances of several tens of pc. Spitzer observations of excesses above those photospheres are indicative of dust located at a range of orbital separations, from analogs of the terrestrial zone, to the gas-giant zone, to the Kuiper belt zone in our own Solar System. Such observations are important in the search for exo-solar planetary systems – either those in formation from primordial dust and gas disks, or those which later perturb planetesimals into crossing orbits that collisionally cascade to produce dusty debris disks. For a given system, the mass in small grains to which Spitzer is sensitive is first expected to decrease with time as planet formation begins, then increase on a relatively rapid time scale (few Myr) as the debris phase begins, and finally decrease on a much longer time scale (many Gyr) as the disk slowly grinds itself down and grains are removed via radiative and mechanical effects.

With the goal of understanding how common or rare the evolutionary path taken by our Solar System might have been, we have initiated a Spitzer survey of F–G–K (solar-type) stars. First, we study the formation of planetary embryos in a survey of post-accretion circumstellar dust disks. We aim to understand the evolution of disk properties (mass and radial structure) and dust properties (size and composition) during the main phase of planet-building and early solar system evolution from 3–100 Myr. Second, we study the growth of gas giants in a sensitive search for warm molecular gas at the level of $> 2 \times 10^{-4} M_{\odot}[H_2]$ at 70–200 K, in a sub-sample of the targets from our dust disk survey. Our goal is to constrain directly the time available for embryonic planets to accrete gas envelopes. Third, we investigate mature solar system

evolution by tracing 100 Myr to 3 Gyr old dust disks generated through collisions of planetesimals. Through our analysis we hope to infer the locations and masses of giant planets $> 0.05 M_{\text{Jupiter}} \approx 1 M_{\text{Uranus}}$ through their action on the remnant disk.

Our large sample enables us to measure the *mean properties* of evolving dust disks and discover the *dispersion* in evolutionary time scales. Further, we can search for relations between inferred dust evolutionary path and stellar properties such as metallicity and multiplicity. In the following subsections we detail our science strategy.

2.1. Formation of Planetary Embryos

Our experiment begins as the disks are making the transition from optically thick to thin, the point at which all of the disk’s mass first becomes detectable through observation. The FEPS goals are to:

- constrain the initial structure and composition of post-accretion, optically thin disks;
- trace the evolution of disk structure, composition, and mass over time;
- characterize the time scales over which primordial disks dissipate and debris disks arise;
- measure changes in the dust particle size distribution due to coagulation of interstellar grains at early stages and shattering associated with high-speed planetesimal collisions at later early-debris stages;
- infer the presence of newly formed planets at orbital radii of 0.3-30 AU.

Photometric observations from 3.6-160 μm with Spitzer probe temperatures (radii) encompassing the entire system of planets in our Solar System. In Figure 1 we show the mass sensitivity of Spitzer as a function of wavelength, indicating the mass in small grains that Spitzer can detect as a function of orbital radius. Detailed spectrophotometry in the range 5.3–40 μm permits a search for gaps in disks caused by the dynamical interaction of young gas giant planets and the particulate disk from 0.2–10 AU. This extends from just outside the innermost radii of the exo-solar “hot Jupiters” (thought to have suffered significant orbital migration in a viscous accretion disk) to the gas giants of our Solar System (thought to have formed beyond the “ice line”).

Mid-infrared spectroscopic observations are sensitive to dust properties including size distribution and composition. They thus probe physical conditions in the disk. From observations in the 5.3–40 μm spectral region we determine the relative importance of broad features attributed to amorphous silicates (ubiquitous in the ISM) compared to numerous narrow features due to crystalline dust (observed only in circumstellar environments). In this way, we can look for evidence of, e.g. radial mixing in the disk since the temperature required to anneal grains ($> 1000\text{K}$) is substantial higher than that inferred for the continuum emitting material ($\sim 300\text{K}$). Further, the shape and strength of specific mid-infrared spectroscopic features provide constraints on the fractional contribution of each grain population to the total opacity, necessary for estimating dust mass surface densities (see section 4.2).

2.2. Growth of Gas Giants

Next, we have undertaken the most sensitive survey to date of atomic and molecular gas in post-accretion disk systems. In order to characterize gas dissipation and to place limits on the time available for giant planet formation we obtain high spectral resolution ($R=600$) data from 10–37 μm with the IRS of 35 stars selected

from our dust disk survey sample. The data include the S(0) 28.2 μm , S(1) 17.0 μm , and S(2) 12.3 μm H_2 lines as well as strong atomic lines such as [SI] 25.23 μm , [Si II] 34.8 μm , and [FeII] 26 μm (Gorti & Hollenbach 2004; Hollenbach et al. 2005). We focus on the post-accretion epochs from 3–100 Myr to examine whether gas disks persist after disk accretion onto the star has ceased and planetesimal agglomeration has removed the dust disk, potentially providing “nucleation sites” for gas giant planet formation.

Understanding gas–dust dynamics is crucial to our ability to derive the time scales important in planet formation and evolution. The dust and gas experiments being conducted at young ages (<100 Myr) have an important synergy in furthering this understanding because dust dynamics are controlled by gas drag rather than radiation pressure when the gas-to-dust mass ratio is >0.1 , while it is the presence of dust that mediates gas heating and therefore detectability. If the gas to dust ratio is low (the dust opacity per gas particle high) and the gas and dust are at similar temperatures, the detection of gas lines by Spitzer becomes difficult due to the small ratio of line to continuum. However, the theoretical models of Gorti & Hollenbach (2004) show that in many instances the dust opacity is sufficiently low and the gas temperature sufficiently high (> 100 K) that small quantities ($< 0.1 M_J$) of gas, if present, can be detected by Spitzer around nearby disks with optically thin dust (see section 4.4).

2.3. Mature Solar System Evolution

Finally, we conduct a study of second generation “debris disks”. The presence of *any* observable circumstellar dust around stars older than the maximum lifetime of a primordial dust disk (the sum of the to-be-determined gas dissipation time scale and the characteristic Poynting–Robertson drag time scale) provides compelling evidence not only for large reservoirs of planetesimals colliding to produce the dust, but also for the existence of massive planetary bodies that dynamically perturb planetesimal orbits inducing frequent collisions.

We have undertaken the first comprehensive survey of F5–K5 stars with ages 100 Myr to 3 Gyr that is sensitive to dust disks comparable to those characteristic of our own Solar System throughout its evolution. We chart the history of our Solar System from 100–300 Myr, the last phase of terrestrial and ice giant ((Uranus- and Neptune-like) planet–building, through 0.3–1 Gyr, bracketing the “late heavy bombardment” impact peak which might have had an effect on the early evolution of life on Earth, and finally over 1.0–3.0 Gyr, examining the diversity of evolutionary paths among mature planetary system. Spectroscopic observations in the range 5.3–40 μm enable diagnosis of gaps caused by giant planets and estimates of dust size and composition which translate directly into constraints on the mass opacity coefficients for the dust (Miyake & Nakagawa, 1993) as well as Poynting–Robertson drag time scales (Backman & Parsec, 1993).

3. Survey Preparation and Execution

3.1. Observing Strategy

A complete and uniform set of Spitzer photometric and spectroscopic observations are obtained for all stars in our dust disk evolution sample, as described below. To derive statistically meaningful results on the disk and dust properties, we observe ~ 50 stars in each of 6 logarithmically spaced age bins from 3 Myr (connecting our Legacy program to that of Evans et al.) to 3 Gyr (beyond which there is strong emphasis by GTOs on debris disk science; Beichman et al. 2005). Our targets span a narrow mass range (0.7–2.2 M_\odot)

and are proximate enough to enable a complete census for circumstellar dust comparable to our model solar system as a function of age. We measure the stellar photosphere at $\text{SNR} > 30$ for λ 3.6–24 μm , $\text{SNR} > 5$ at 70 μm (or $\text{SNR} > 5$ for $5 \times$ the current zodiacal dust emission) with broadband photometry from IRAC and MIPS (subject to calibration uncertainties). To identify gaps in the dust distribution created by the presence of giant planets from 0.2–10 AU, we require relative spectrophotometry with $\text{SNR} > 30$ from 5.3–11 μm , and with $\text{SNR} \sim 6$ –12 at wavelengths between 20–30 μm with the IRS.

A sub-sample of 35 stars comprises our gas disk evolution study with the high resolution mode of the IRS. This sample spans a range of spectral type (F3–K5), age (3–100 Myr), activity ($L_x/L_{bol} \sim 10^{-3} - 10^{-5}$), and a wide range of infrared excess emission, with some preference for optically-thin excess in the mid-infrared. Fourteen stars were chosen for first-look observations and enable us to explore the limits implied by null results and guide our choice of follow-up observations for additional stars drawn from our dust disk survey.

Our goal is to collect data capable of realizing the fundamental limits imposed by instrument stability and systematic calibration uncertainties. Integration times are chosen according to each star’s distance, age and spectral type to reach uniform SNR at the photospheric limits, as specified above – thereby providing a *complete census* of dust disks for our targets.

3.2. Sample Selection

The source list for FEPS consists of young near-solar analogs, stars ranging in mass from 0.7–2.2 M_\odot though strongly peaked at 1 M_\odot (see Figure 2), and spanning ages 3 Myr to 3 Gyr (our Sun is 4.56 Gyr old). The stars are drawn from three recently assembled samples.

First, Soderblom et al. (1999) have produced a well-characterized set of ~ 5000 solar-type stars spread over the entire sky (see also Henry et al. 1996) having parallaxes that place the stars within 60 pc, (B–V) colors between 0.52 and 0.81 (F8–K0 spectral types), and location in the Hertzsprung–Russell diagram within 1.0 mag of the solar-metallicity Zero-Age Main Sequence. This sample is fully complete out to 50 pc. The age distribution in such a volume-limited region around the Sun is roughly flat in linear age units out to 2.5 Gyr, at which point heating by the Galactic disk has increased the scale height of older stars and thus removed them from the volume-limited sample. From this catalog we have selected a sample with ages based on the R'_{HK} chromospheric activity index from ~ 100 Myr to 3 Gyr. However, being located more than 100 pc from the nearest sites of recent star formation, the immediate solar neighborhood is deficient in stars with ages younger than 100 Myr. Hence the volume limit was extended in order to identify large enough samples of young stars for the FEPS project.

We have conducted a new (e.g. Mamajek et al., 2002) and literature-based examination to identify stars whose ages are in the range 3–100 Myr. These were selected as having (B–V) colors between 0.58 and 1.15 or spectral types G0–K0, strong x-ray emission, kinematics appropriate for the young galactic disk, and high lithium abundance compared to the 120 Myr old Pleiades. Young stars are copious coronal x-ray emitters and a large body of literature demonstrates the connection between x-ray emission, chromospheric activity, stellar rotation, and age. The surface density distribution of x-ray sources detected by the ROSAT all-sky survey reveals a concentration of objects coincident with Gould’s Belt, a feature in the distant solar neighborhood (50–1000 pc) comprised of an expanding ring of atomic and molecular gas of which nearly all star-forming regions within 1 kpc are a part. These x-ray sources are thought to be the dispersed low-mass counterparts to a series of 1–100 Myr-old open clusters and extant and fossil OB associations that delineate Gould’s Belt (e.g. Torra et al. 2000; Guillout 1998). Proper motion data enable us to select the nearest

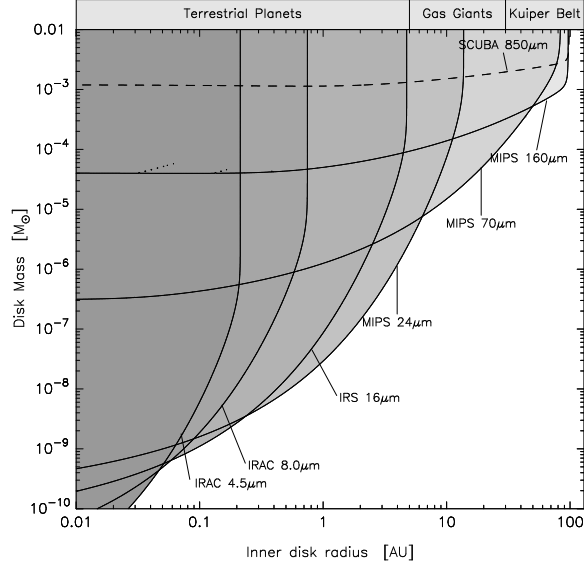


Fig. 1.— Spitzer sensitivity to mass in small grains as a function of radius in a hypothetical circumstellar disk surrounding a sun-like star at a distance of 30 pc for integration times typical for FEPS. For emission from small grains in radiative equilibrium, each radius in the disk corresponds to a specific dust temperature. From simple blackbody considerations, shorter Spitzer wavelengths probe warmer dust (at smaller orbital radii) while longer Spitzer wavelengths probe cooler dust (at larger orbital radii), as indicated.

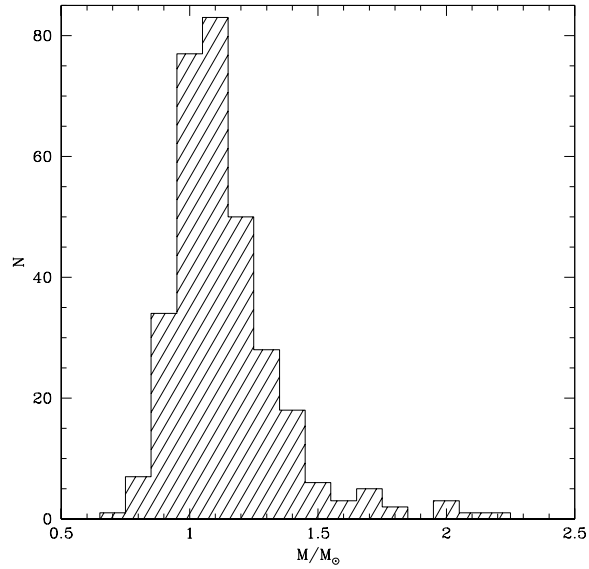


Fig. 2.— Distribution of masses for stars in the FEPS sample. The range spans 0.7–2.2 M_{\odot} though it is strongly peaked at 1.0 M_{\odot} .

of these young, x-ray-emitting stars with space motions consistent with those of higher mass stars having measured parallax, and hence estimate their distances. Follow-up optical spectroscopy of these x-ray + proper motion selected stars is used to confirm youth and determine photospheric properties. A total of ~ 600 field stars are x-ray-selected candidate young stars.

Finally, stars in nearby well-studied open clusters [IC 2602 (55 Myr), Alpha Per (90 Myr), Pleiades (125 Myr), Hyades (650 Myr)] serve to “benchmark” our field star results by providing samples nearly identical in age, composition, and birth environment. We considered all known members of these clusters meeting our targetted mass / B-V color / spectral type range that were not part of GTO samples.

From this large parent sample, stars were selected for potential observation with Spitzer if they met all of the following additional criteria. The criteria were chosen to ensure sufficient signal-to-noise on the stellar photosphere out to $24\ \mu\text{m}$ with Spitzer and thus accurate characterization of the underlying photosphere both observationally and with stellar models.

- $K < 10$ mag (young < 100 Myr x-ray selected and cluster samples) or $K < 6.75$ mag (older 0.1-3 Gyr Hipparcos + R’HK selected sample)
- $24\ \mu\text{m}$ background $< 1.70\ \text{mJy/arcsec}^2$ (x-ray selected samples) or $< 1.54\ \text{mJy/arcsec}^2$ (Hipparcos + R’HK sample)
- $70\ \mu\text{m}$ background $< 0.76\ \text{mJy/arcsec}^2$
- galactic latitude $|b| > 5^\circ$ (stars in IC 2602 were permitted to violate this criterion)
- quality 2MASS JHK photometry, with no flags
- no projected 2MASS companions closer than $5''$
- no projected 2MASS companions closer than $15''$ unless they are *both* bluer in J-K *and* fainter in K by > 3 mag than the Spitzer target.

These criteria were applied uniformly to our parent sample though in the cases of a few exceptional stars (such as the IC 2602 sample) some criteria were violated. Next, targets appearing on Spitzer GTO programs were removed from the source list. Also, to a limited degree, stars identified through spectroscopy or high resolution imaging literature published through March 2001 as being binary, with companions closer than $2''$, were removed. These cases were all either spectroscopic binaries or visual binaries with small delta magnitudes and the literature search was not exhaustive. Subsequent investigation using AO imaging have uncovered additional binary systems with larger delta magnitudes remaining within the FEPS sample (e.g. Metchev & Hillenbrand, 2004).

Finally, amongst the stars in our parent sample older than ~ 600 Myr, approximately 1/2 were arbitrarily removed from our program in order to even out the age bins and bring the observing program within the allocated number of Spitzer hours (350).

Based on pre-Spitzer spectral energy distributions assembled from the literature, 2MASS, IRAS, ISO, and ancillary observations conducted to date, several (5-7) of the youngest stars in our program show some hint of circumstellar material. Because the stars were randomly selected based on their kinematic and activity properties as derived from optical information, these previously known dust excesses do not bias the program.

To this source list a set of 14 stars was added, which were suspected to have optically thin dust excesses based on observations from IRAS and ISO. These stars formed part of our first-look gas disk detection survey and should not be used to derive the statistics of dust debris as a function of age.

Our final target list for observations with Spitzer and ground-based ancillary programs consists of 328 solar-type stars distributed uniformly in log-age between 3 Myr and 3 Gyr. Approximately 60 of these are members of the open clusters IC 2602, Alpha Per, Pleiades or Hyades. The remainder are field stars distributed in distance between 11 and 180 pc. The relation between distance and age for this sample is shown in Figure 3. The complete source list is presented in Table 1 (field stars), Table 2 (open cluster stars), Table 3 (young stars), and Table 4 (pre-selected IRS high resolution targets). The names, coordinates, and spectral types are those found in the Spitzer Legacy Science Archive (<http://ssc.spitzer.caltech.edu/legacy/all.html>) and details will be presented in Hillenbrand et al. (in prep).

3.3. Spitzer Data

3.3.1. Astronomical Observing Requests

FEPS uses all three science instruments on board Spitzer to provide data from $3.6\ \mu\text{m}$ to $70\ \mu\text{m}$ (with a subset of the FEPS stars also observed at $160\ \mu\text{m}$) including $\lambda \sim 7 - 38\ \mu\text{m}$ low resolution IRS spectra. A detailed description of the observing commands (Astronomical Observing Requests or AORs) that specify the FEPS program can be found using the SSC’s SPOT software to “View Program” and entering Program Identification Number (PID) 148. In this section we outline the AOR strategy for each instrument.

Data are obtained with IRAC in three bands (3.6 , 4.5 , and $8.0\ \mu\text{m}$). The first five FEPS objects observed as part of the early verification program were observed in all four IRAC bands (including the $5.6\ \mu\text{m}$ channel). FEPS stars are observed in the IRAC Subarray mode (32×32 pixels) at frame-times of 0.02, 0.1, or 0.4 seconds, using the “4 point-random” dither pattern at the medium dither scale. At each of the 4 dither positions, 64 images are taken at the same frame-time in each band. Thus there are 256 images of each star for each IRAC band.

Low resolution ($R \approx 64\text{--}128$) spectra covering the longer wavelength ranges ($7.4\text{--}38\ \mu\text{m}$) in the SL1, LL1, LL2 modules of the IRS are obtained for all FEPS objects. Observations using the SL2 module ($5.2\text{--}7.7\ \mu\text{m}$) were also obtained for the five validation stars and for objects younger than 30 Myr. High resolution ($R \approx 600$) spectra are obtained for the 35 stars chosen for the gas detection experiment. All IRS observations use standard starrng mode, and high accuracy peak-up.

MIPS photometric imaging data at 24 and $70\ \mu\text{m}$ are obtained for the entire FEPS sample. We achieve $\text{SNR} > 30$ at $\lambda \leq 24\ \mu\text{m}$ for our entire sample and $\text{SNR} > 5$ at the photospheric limit for as much of our sample as practical at $\lambda = 70\ \mu\text{m}$. For sources whose photospheres we are unable to detect in a reasonable time (10 cycles), we achieve $\text{SNR} > 5$ on dust debris at $\times 5$ current Solar System values. MIPS $160\ \mu\text{m}$ data are also obtained for 10% of the lowest background targets, chosen to span the age range of the full sample. The MIPS default scale photometric mode acquires data in multiple pointings with small offsets between each pointing to alleviate instrumental artifacts and cosmic rays. Due to the stability of the Si:As array, these multiple pointings for the $24\ \mu\text{m}$ data allow repeatability to be used as an accurate estimate of internal measurement (precision) uncertainty. For 70 and $160\ \mu\text{m}$, the multiple pointings are used to calibrate the time-dependent detector response, and therefore only a final mosaic image is produced by the photometry mode for the Ge:Ga arrays.

3.3.2. Data Reduction

The SSC pipelined data products from FEPS can be accessed through the SSC’s LEOPARD archive browser. In this section we outline the general data reduction strategy for each instrument. We refer the reader to FEPS data publications for more detailed description of the data reduction applied to individual sources (see also the FEPS Explanatory Supplements that accompany our data releases through the Spitzer Science Center).

IRAC

IRAC data frames are processed through the SSC pipeline to produce Basic Calibrated Data (BCD) images. Sixty four images are obtained at each of the four dither positions for a total of 256 images of the object, in each band.

Flux densities are derived using aperture photometry. A Gaussian fit to the PSF is used to center the target aperture. The target and background annuli are optimized for the ensemble of observations to maximize the measured SNR. These measured flux densities are then corrected to the standard calibration aperture sizes supplied by the SSC. To estimate measurement uncertainties we assign the standard deviation of the 256 measurements as the one-sigma (1σ) internal uncertainty. The total uncertainty reported by FEPS is the (square-) root of the sum of squares (RSS) of this internal measurement uncertainty and the calibration uncertainty as published by the SSC. Although the calibration of IRAC assumes a flat ($\nu F_\nu = \text{const.}$) spectrum across the band-pass, no color corrections have been applied to the FEPS IRAC measurements. The prescription for color-corrections is presented in the IRAC Data Handbook available through the SSC.

IRS

IRS data are first processed through the SSC pipeline to remove instrumental artifacts including dark current, droop signal and flat field structures. From these pipelined data we proceed with the intermediate ”droopres” data product. The SMART reduction package developed by the IRS Instrument Team at Cornell (Higdon et al 2004) is then used to extract the spectra. As a first step, we correct for the background emission and stray-light by subtracting the images obtained from the two slit positions at which a object is observed for each module and order (automatically in standard starring mode). This results in a set of images containing a positive and negative spectrum in each observed order. Before extraction, all hot or dead pixels in each image are replaced.

For the spectral extraction we use a straight-sided (boxcar) aperture limiting the extraction area around the positive source in the background corrected images. Since all observations in the FEPS legacy program use high accuracy peak-up and the pointing of Spitzer is good to within 0.4” radius (1σ), we fix the position of the aperture in each spectral order. The width of each aperture is chosen such that 99% of the source flux is within the aperture for all wavelengths in the order. A mean spectrum over all slit positions and cycles is computed for each individual order from the spectrum for each nod position and cycle. The orders are then combined. The quoted uncertainties are the 1σ standard deviation of the distribution of data points used to calculate the mean spectrum over all cycles and nod positions, modified to include the errors of the photometric calibration. Finally, the orders are stitched together with unit weight by taking the mean flux at overlapping wavelength points.

MIPS

MIPS data were originally reduced using the Data Analysis Tool developed by the MIPS Instrument Team at the University of Arizona (Gordon et al. 2004), since the MIPS Instrument team was charged with fast development of the primary reduction algorithms. This package uses the raw data product available from the SSC data archive. Dark subtraction, scan mirror dependent flat field, electronic nonlinearity correction, droop subtraction, and cosmic ray rejection are applied. For the final FEPS releases, the SSC pipeline products are used, since the combined efforts of the Instrument Team at the University of Arizona have been successfully implemented at the SSC and the two reduction schemes have converged on a common, validated product.

Flux densities for each band are derived from aperture photometry. The position of the aperture was found by fitting a two-dimensional Gaussian to the core of the PSF when the object is detected. For non-detections, as is often the case for 70 and 160 μm , the aperture is centered on the object coordinates. Aperture correction factors are applied to match the “infinite aperture calibration” defined by the MIPS Instrument Team (MIPS Data Handbook).

We use the standard deviation of the photometry from the stack of individual dither images (24 μm), or the RMS noise in the background propagated over the pixels in the object aperture as estimates of the random photometric uncertainty (70 and 160 μm). Total uncertainties are the RSS of the internal uncertainties and the published calibration uncertainties. As for IRAC, color-corrections are not applied. However, we note that the MIPS team assumes a 10,000K black-body for its calibration (MIPS Data Handbook).

3.3.3. Verification and Validation

Quality control is applied to the Spitzer observing program as follows. All observations are verified, meaning checks on whether the correct source was observed, in the requested instrument mode, and following the prescribed AOR. The observations are further validated by considering photometric uncertainties derived from the observations compared with theoretical uncertainties based upon expected photon count rates and other known noise sources such as extragalactic confusion at 70 and 160 μm . Expected versus derived SNRs are assessed for observations at wavelengths where the measured flux densities are consistent with being photospheric. Comparison with photospheric model expectations enable us to investigate systematic offsets in expected versus observed fluxes as a function of source color and brightness, although we are unable to unambiguously separate errors in the models from errors in the data. For wavelengths $\lesssim 24 \mu\text{m}$, the exposure times were sufficient to measure the photospheric emission with expected $\text{SNR} > 30$. We also verify that fluxes derived from different instruments over common wavelength ranges agree within the errors. Further details can be found in the Explanatory Supplements that accompany our data release through the Spitzer Science Center.

3.4. Ancillary Data

In addition to the Spitzer observations, we are engaged in a rich ancillary observing program that both complements and aids our interpretation of the Spitzer spectrophotometry. These data include ground-based 10 μm , sub-millimeter, and millimeter photometry, an echelle spectroscopic survey for photospheric characterization, and an adaptive optics imaging survey for companion detection and characterization.

Dust Mass Constraints: We have engaged in a limited ground-based mid-infrared campaign on a few tens of FEPS targets. Imaging photometry at $10\ \mu\text{m}$ of selected members of the FEPS sample were obtained with LWS on the Keck I telescope and SpectroCam-10 (SC-10) on the Hale 5-meter telescope (Metchev et al. 2004) and also with MIRAC3 on the Magellan I telescope (Mamajek et al. 2004). The observations were largely consistent with photospheric emission with few exceptions where excess emission was detected, indicative of terrestrial zone dust. We also searched for dust located at larger radii and hence too cold to radiate strongly in the MIPS $160\ \mu\text{m}$ band. We obtained sub-mm and/or mm continuum observations for approximately 1/3 of our sample. Millimeter observations were obtained using the Owens Valley Radio Observatory (OVRO) millimeter-wave interferometer at $3.1\ \text{mm}$ or the 37-element SIMBA bolometer camera on the 15m Swedish-ESO Submillimetre Telescope (SEST) at $1.2\ \text{mm}$, for a total of 89 stars. Submillimeter observations at $350\ \mu\text{m}$ were obtained for 6 stars using the SHARC bolometer camera on the 10.4m telescope of the Caltech Submillimeter Observatory (CSO). These observations are discussed in detail by Carpenter et al. (2005). Thirteen FEPS sources were observed by Najita and Williams (2005) at the James-Clerk-Maxwell Telescope (JCMT) using SCUBA. The sources were selected with an emphasis on those that are young (10 Myr to 300 Myr) and nearby ($< 50\ \text{pc}$). Three sources were detected including HD107146 (Williams et al. 2004).

Gas Mass Constraints: As a complement to our Spitzer H_2 program we are attempting CO rotational transition detection at millimeter wavelengths with OVRO, Sub-millimeter Telescope facility of the Arizona Radio Observatories, and the JCMT, as well as fundamental vibrational emission at mid-infrared wavelengths ($4.5\ \mu\text{m}$), and the pure rotational transitions of H_2 at $17\ \mu\text{m}$. A sample of ~ 20 sources were observed in the CO(2-1) line with the SMT and upper limits were derived. These data are being combined with Spitzer observations and results are reported in Pascucci et al. (2006). In addition, Najita and Williams (2005) have searched for CO(3-2) emission from two of the submillimeter excess sources and place limits on the gas mass in these systems. In the case of HD107146, a conventional analysis suggests that the upper limit on the gas-to-dust ratio is much less than primordial.

Age Diagnostics: An important aspect of our program is determination of the tightest constraints possible on the ages of our sources (Hillenbrand et al. in preparation). To do so we consider a number of diagnostics related to activity, which generally decreases with increasing stellar age, or elemental abundances, in particular Li I. We have assembled all x-ray information from the ROSAT archives. We have R'_{HK} indices for over 3/4 of our sample, from the literature or newly measured from our ancillary high dispersion ($R \approx 20,000$ from $3600\text{--}9500\text{\AA}$) optical spectra. In addition to Ca II H&K core emission line strengths, we are also measuring $\text{H}\alpha$ emission/absorption equivalent widths, Li I equivalent widths, and rotational velocities, all of which change with stellar age. A full discussion of stellar age indicators and their likely uncertainties is beyond the scope of this paper (cf. Hillenbrand et al.). However, we find generally that when multiple age indicators are available for a given star they agree with one another to better than 0.5 dex in log-age. This level of accuracy is adequate for investigating general trends in debris disk evolution. Finally, we can also derive effective temperatures, gravities, and metallicities for each star through spectral synthesis modelling.

Stellar, Sub-stellar, and Planetary-mass Companions: In order to place our own Solar System fully in context, we must consider the effects of stellar multiplicity at the same time we are considering dust disk evolution. Our Sun's planets exist at orbital radii ranging from 0.4-30 AU with the Kuiper Belt extending out to at least 50 AU, and our Sun is not a member of a multiple star system. A significant fraction (30-80%) of all sun-like stars do appear to be born in multiple star systems (binaries, triples, quadruples; Mathieu et al. 2000) and, as shown for solar-type, solar-neighborhood multiples by Duquennoy & Mayor (1991), the distribution of orbital periods is lognormal and peaked at 180 days or 30 AU – i.e. within our current Solar

System. Searches for companions (stellar, sub-stellar, and planetary-mass) to members of our Spitzer sample via both high resolution imaging and spectroscopy are underway, in order to assess the role of multiplicity in disk evolution.

With the adaptive optics (AO) at the Palomar 200" we have observed every northern star on our program with short JHK_s exposures, designed to detect bright companions as close as 0.1" (5 AU for sources at 50 pc). Such companions within the Spitzer beam (5" at 24 μ m) are critical to account for when analyzing spectral energy distributions. For a selected subset of our stars we are also performing deep K_s-band AO coronagraphy designed to detect much fainter companions. Due to evolution of the mass-luminosity relationship and contrast limit, there is an intricate grid of tradeoffs in the companion mass detection limit as a function of system age and orbital separation, with sensitivity to lower masses achievable at younger ages and larger separations. In the case of our target list, we are sensitive to masses as low as 3-10 $M_{Jupiter}$ (for example, at separations of 2" to $\Delta K = 13$ mag at SNR = 5). Follow-up proper motion, photometry, and spectroscopy is conducted with the Palomar 200" and with Keck (e.g. Metchev & Hillenbrand, 2004; 2006, in press).

High dispersion spectroscopy is also being used to identify companions. Several double-line or single-line spectroscopic binaries have been found from our Palomar 60" echelle spectroscopy (White et al., submitted). Further, at least 25% of our Spitzer target stars are located on various radial velocity planet search programs, a number of which are already known to have planetary companions or will be found with planetary companions over the next decade. Several FEPS targets are also being monitored photometrically in order to derive rotation periods from star-spot activity on the stellar surface.

4. Supporting Theoretical Framework

Physical theories are needed to guide our observational program and to help interpret the results. The basic problem is to understand the formation and evolution of planetary systems based on observed spectral energy distributions, and spectroscopic observations. In support of this work, we have undertaken a limited modeling effort aimed at constraining: 1) basic disk properties utilizing a minimum of assumptions; 2) the amount of remnant gas in disks based on IRS high resolution spectra; and 3) the diversity of planetary architectures based on estimates of geometric dust distributions derived from the SEDs.

4.1. Toy Model for Solar System Evolution

We start with a basic model of the evolution of our own solar system. As is well known, our planetary system contains two major debris belts: the Kuiper Belt and the Asteroid Belt, both of which are generating dust through mutual collisions of larger parent bodies. Figure 4 shows the dust mass and the observed SEDs predicted by two plausible models for the evolution of our Solar System from 100 Myr to 4.5 Gyr, as viewed from 30 pc. The models assumes only a minimum mass solar nebula and planetesimal scattering and collision frequencies according to two simple analytic representations: one (bottom) including the effects of dynamical instability postulated to have removed a large fraction of dust-producing parent bodies in the asteroid and Kuiper Belts in our Solar System (Gomes et al. 2005; see also Strom et al. 2005) and the other (top) excluding those effects. In the former case, dust production diminishes linearly in time as expected for a high density planetesimal belt in collisional equilibrium where dust is ultimately removed through radiation pressure blowout of the smallest fragments (Dominik and Decin, 2003; Wyatt, 2005) until the instability

occurs at approximately 500–600 Myr. In the latter case, the belt grinds itself down to the low density limit where dust removal is dominated by P–R drag and the dust mass observed decays at t^{-2} . In the absence of this instability, our hypothetical solar system is detectable by Spitzer with IRAC (zodiacal dust disk) and MIPS (Kuiper disk) from 30 pc at age 100 Myr, while only the Kuiper belt dust would be found at an age of 4.5 Gyr. In this way, we can attempt to address whether or not our Solar System is common or rare compared to typical stars in the disk of the Milky Way galaxy. Details concerning this model can be found in Meyer et al. (2006).

One deficiency in this model is neglecting the drag on orbiting grains due to stellar winds. Azimuthal wind drag could dominate radiation P–R drag for the high mass-loss rates expected from young solar-type stars (Jura 2004). This would decrease grain lifetimes in systems that are P–R drag dominated, and diminish the number of systems thought to be collisionally dominated. However, recent work (Wood et al. 2005) suggests that the large effects suggested in earlier work (Wood et al. 2002) may have been overestimated. While this effect can be important, its magnitude is still uncertain.

4.2. Constraints on Dust Properties

The observed SEDs from dust disks are determined in part, by the optical properties of the dust contained therein. Both particle size and composition are important in determining the absorption and emission properties of the dust, thus determining its temperature for a given distance from the central star. In the absence of constraints on dust properties from spectral features, resolved images of disks in thermal emission or scattered light, or far-IR/sub-mm spectral slopes, models to explain the observed SEDs of debris disks are necessarily degenerate (see for example Hines et al. 2006). Spectroscopic observations of solid state features can provide important constraints on physical models for the dust. For example, large particles ($a_{DUST} > \lambda_{resonance\ feature}/\pi$) are not efficient radiators at their natural resonance frequencies. Thus the absence of expected solid state features from abundant species can indicate a minimize grain size. Similarly, specific chemical compositions of dust can change the shape and central wavelength of resonance features, or indicate significant structural differences in the dust (e.g. amorphous versus crystalline silicates). Discerning the difference between Mg- and Fe-rich end member silicates and fractions of amorphous to crystalline silicates provide crucial information concerning the chemical properties of the nebula in which parent body planetesimals formed, as well as the processing history of the dust. Detailed models exploring these effects are described in Wolf & Hillenbrand (2003) and Bouwman et al. (in preparation).

4.3. Dynamics of Disk–Planet Interactions

As part of our theory effort we have developed numerical tools to model debris disks originating from an outer belt of planetesimals and evolving under the effect of gravitational perturbation from giant planets in various planetary configurations and for different dust particle sizes and compositions (Moro-Martín & Malhotra, 2002; Moro-Martín & Malhotra, 2003; and Moro-Martín et al. 2005). Even though the particle dynamics is chaotic, our method can robustly estimate the equilibrium radial density distribution of dust. The dust density structure carved by giant planets affects the shape of the disk SED, in a manner that depends upon the the mass and location of the perturbing planet as well as the grain properties (chemical composition, density and size distribution). We found that the SED of a debris disk with embedded giant planets is fundamentally different from that of a disk without planets, the former showing a significant

decrease of the near/mid-IR flux due to the clearing of dust inside the planet’s orbit. The SED is particularly sensitive to the location of the planet, i.e. to the area interior to the planet’s orbit that is depleted in dust due to gravitational scattering by the planet. Our dynamical models show that for a planet in a circular orbit with semimajor a_{pl} , the radius of the depleted inner zone is in the range of $0.8\text{--}1.2 \times a_{pl}$ depending upon the planet mass. Our models also show that the dust depletion factor (i.e. the ratio between the dust density inside and outside the depleted region) depends significantly on the planet mass when the mass is in the range $1M_{Nep} < M_{pl} < 3M_{Jup}$. However, there are two issues that complicate the interpretation of the SED in terms of planet location: (1) The SEDs are degenerate. In particular, there is a degeneracy between the dust grain chemical composition and the semimajor axis of the planet responsible for inner the gap. For example, the SED of a dust disk dominated by weakly absorbing grains (Fe-poor silicate) has its minimum at wavelengths longer than those of a disk dominated by strongly absorbing grains (e.g. carbonaceous and Fe-rich silicate), which may be mistaken by the presence of a larger inner gap. This degeneracy can be resolved either with high resolution spectroscopy (which would constrain the grain chemical composition as discussed above), or high spatial resolution images (which would spatially resolve the inner edge of the dust disk). (2) Because of the Spitzer sensitivity limit, the debris disks observed by FEPS may be in the collision-dominated regime, where the dynamics of the dust particles are dominated by collisions rather than P-R drag (Dominik & Decin, 2003; Wyatt, 2005). This may result in the dust particles suffering multiple collisions, that could break them down into smaller and smaller grains until they are blown out from the system by radiation pressure, before they have time to migrate from the dust-producing planetesimals to a planet-crossing orbit.

4.4. Models of Gas in Disks

In order to interpret our high resolution spectroscopic observations of gas in disks from ages of 3 Myr to 100 Myr, we have developed detailed thermo-chemical models of gas and dust in optically thin disks (Gorti & Hollenbach 2004). Our models calculate the gas spectral line emission and dust continuum emission for comparison with observed data and thereby infer disk properties. The models calculate the gas and dust temperatures separately, assuming a balance between the heating and cooling processes. We include various heating sources for the gas, such as collisions with warm dust heated by stellar radiation, X-rays, exothermic chemical and photo-reactions, cosmic rays and grain photoelectric heating. The gas cools by ionic, atomic and molecular line emission. The disk temperature structure, vertical density structure, and chemistry is self-consistently calculated in our disk models by requiring thermal balance, vertical pressure equilibrium and by assuming steady-state chemistry. Our chemical network consists of 73 ionic, atomic and molecular species involving H, He, C, O, Si, Mg, Fe and S and 537 reactions. Inputs to our models are stellar parameters such as the radiation field at X-ray, UV and visible wavelengths, the disk surface density distribution in gas and dust, and dust properties (chemical composition and size distribution). Most of the stellar and dust parameters are determined through ancillary observations and by modeling of the dust continuum observed through the FEPS program. For a given dust and gas surface density distribution, our theoretical models can predict the spectral line emission from the gas and the dust continuum emission for comparison to observations.

We are in the process of developing similar gas disk models for younger, optically thick dust disks. We use a two-layer model for the dust temperature calculation (Chiang & Goldreich 1997), and adopt a procedure similar to that for optically thin disks for the gas temperature. The gas and dust temperature are calculated separately and the emergent line plus continuum spectrum computed.

Spitzer IRS in the high resolution mode is capable of detecting (3σ) warm gas ($T_{gas} \sim 100$ K) masses of $\lesssim 0.2M_J$ in disks at distances of 160 pc or less (Gorti & Hollenbach 2004). The FEPS H₂ program will measure spectral line fluxes (or upper limits to line fluxes) and these will be compared with the gas models to infer the gas masses in disks and the spatial distribution of gas (e.g. Hollenbach et al. 2005; Pascucci et al. 2006).

5. Analysis Plan

Our approach to analyzing the data collected as part of FEPS starts with as few assumptions concerning the physical nature of the observed system as possible, and proceeds to more elaborate models concerning the excess emission. At each stage, additional assumptions are made which enable a richer interpretation of the data. However, the certainty of our conclusions diminishes as we proceed. In any event, we attempt to clearly state our assumptions as we go, and try to be careful not to proceed on the basis of assumptions that are demonstrably false. In following this analysis procedure, it is important to always keep in mind how the results depend on the input assumptions, as well as explore the full range of model parameters allowed by the data, including the uncertainties.

Emission in excess of that expected from the stellar photospheres is found by subtracting model photospheric flux estimates from the observed fluxes across the wavelength range accessible to Spitzer. We execute the following generic analysis for all sources with excess emission of 5σ or greater at one or more wavelengths, or equivalent detections of lower SNR but at two or more wavelengths. We begin by calculating an approximate dust temperature if the excess is detected at two or more wavelengths. If the excess is detected at only one wavelength, we derive a temperature limit using the excess and the bluest broadband point without excess. With this temperature fit to the data, we then estimate the ratio of excess luminosity in the infrared to the total stellar luminosity $f \sim f_{IRX}/f_*$.

If the source presents an excess over a broad range of wavelength, we explore whether a range of dust temperatures would be a more appropriate model. Emission that appears to be optically-thick in the direction perpendicular to the disk from the point of view of the observer over a range of wavelength is initially assumed to be a primordial gas-rich disk left over from the formation of the star. If high resolution IRS data are available for the source we can assess whether these observations constrain the amount of molecular gas remnant in the disk. Other observations such as mm-wave CO data or evidence for active accretion onto the star can also suggest a primordial disk. Evidence for a flared disk geometry from the SED can also provide evidence for a gas-rich primordial disk.

If there is no evidence for remnant gas in the disk, we proceed under the premise that the disk might be a debris disk, where the dust we see is generated through collisions of larger parent bodies in a planetesimal belt. Assuming the grains are large, efficient absorbers and emitters of light, we can calculate the required dust cross-sectional area for the emitting grains, and determine a plausible radius in the disk for the planetesimal belt. For an excess observed at a wavelength λ , we can assume that grains larger than λ/π can be treated approximately as perfect blackbodies. Given the luminosity of the star, we can also calculate the radiation pressure blow-out size, providing a bound on the smallest particles that could be responsible for the radiation. To further constrain the grain size distribution and composition, we also search for evidence of solid state emission features in the IRS low resolution spectra obtained for each source. If grains exist in the circumstellar disk at temperatures corresponding to emission at the appropriate wavelength (e.g. 300 K for the 10 μ m silicate feature), the lack of expected spectral features attributed to specific grain compositions can place

constraints on their abundance (e.g. upper limit to the fraction of crystalline silicates in the debris dust) or particle size (grains larger than $\lambda_{solidstatefeature}/\pi$ will not be efficient radiators in the resonance feature) or both. These observations, as well as the observed spectral slope in the far-infrared/sub-mm, constrain the grain size distribution, and thus the range of plausible models for the radii in the disk responsible for the emission at a given temperature. For example, very small grains ($< 0.1 \mu\text{m}$) can reach the same temperature at > 30 AU as very large grains ($> 10 \mu\text{m}$) at < 3 AU (Backman & Paresce, 1993).

Armed with this information, we can calculate basic quantities such as the mass surface density of emitting grains for a given particle size/radius in the disk. This enables us to compare the lifetime of grains of various size under the assumption that they are subject to both mutual collisions in the disk as well as the effects of P–R drag (e.g. Burns et al. 1979). In most cases, observed debris disks have surface densities so high that many collisions will occur between dust grains before they have time to evolve in radius significantly under P–R drag (Dominik & Decin, 2003; Wyatt, 2005). In this case, the grains are eroded down to the blowout size and removed from the system through radiation pressure. If the IR excess is confined to cooler temperatures (and therefore larger radii), we can also place limits on the mass surface density *inside* of R_{inner} and characterize the presence of an inner hole in the dust distribution. In principle, limits on the mass surface density outside of the observed disk radius and R_{outer} could be constrained by FIR and sub-mm observations as well.

In the case where the IR excess is detected with $\text{SNR} > 5$ at several wavelengths, we explore disk model parameters in a robust way by modelling the excess emission and calculating the best-fit by computing the reduced chi-squared metric. Given the number of degrees of freedom in the model, the number of observations, and robust uncertainties in the observations, the reduced chi-squared can provide an estimate of the probability that any parameter lies within a range of values (confidence interval) if the data were drawn from a particular model. As a result we can define *contours* of allowed (correlated) parameters in a multi-dimensional space defined by the model parameters. This requires clearly defined model parameters that can be varied over a range to produce acceptable fits to the data, and clearly defined uncertainties in our data that can be interpreted as errors in a gaussian probabilistic sense.

Even in the absence of robust parameter estimation described above, we can often constrain the family of permitted models or offer a preferred model on the basis of likely physical scenarios and Occam’s razor. For example, in the case where two models match well the observed excess (small grains at large radii vs. large grains at smaller radii), one can argue that the large grain model might be preferred if the surface density of that model were so large as to enable the disk to maintain an inner hole on the basis of mutual collisions down to the blow-out size. The small grain at large radii model might have a surface density so low that an interior planet might be required in order to avoid grains filling in the hole under the action of P–R drag. Thus the large grain model at small radii requires fewer assumptions and might be preferred. Furthermore, we know that T Tauri stars in their youth have optically-thick circumstellar disks from < 0.1 AU that extend to > 30 AU. It might seem implausible to require a massive circumstellar disk composed entirely of small grains $< 1 \mu\text{m}$ at $R > 100$ AU with no evidence for dust or planetesimals inside of 30 AU, rather than a more modest remnant disk composed of larger grains at radii where we know giant planets form and disks exist around sun-like stars (cf. Kim et al., 2005; Hines et al. 2006).

Finally, all of the models considered should make specific predictions that can be tested with follow-up observations. For example, scattered light imaging with adaptive optics on large ground-based telescopes, or utilizing coronagraphy on the Hubble Space Telescope can provide constraints on the radial extent of small grains in the debris disk systems. More sensitive Spitzer observations at mid- and far-IR wavelengths can improve upon low SNR initial detections. Sub-mm observations can constrain disk models, particularly the

use of interferometers to resolve the FIR/sub-mm emission initially detected by Spitzer. In general, having resolved images of disks and one or more wavelengths in thermal emission, or in scattered light break many of the degeneracies associated with SED modelling. For the nearest, youngest systems where a hole in the dust distribution is inferred from SED modelling, we can test those predictions using high contrast imaging techniques to search for warm massive planets in the circumstellar environment $R > 5$ AU. The connection of dust disk emission with the presence/absence of giant planets is still poorly understood (Moro–Martin et al. in press; Beichman et al. 2005) and one of the key goals of the FEPS science program.

6. FEPS Data Products

As part of our commitment to the Spitzer Legacy Science Program, we plan to deliver high quality enhanced data products for the benefit of the community, as well as documentation that will enable archival researchers to utilize these data in the most efficient way possible. In addition to ground-based ancillary data, and the Spitzer database itself, we also provide resources that enable careful scrutiny of the Spitzer calibration, and tools for the research community interested in interpreting observations of debris disk systems.

6.1. Ancillary Data Products

Ancillary data collected in support of FEPS are provided via the published literature and include all data discussed above:

- 10 μm photometry (e.g. Metchev et al. 2004; Mamajek et al. 2004).
- Sub-millimeter and millimeter continuum photometry (e.g. Williams et al. 2004; Carpenter et al. 2005; Najita & Williams, 2005).
- CO gas line measurements or upper limits (e.g. Najita & Williams, 2005; Pascucci et al. 2006).
- Stellar age indices (e.g. Hillenbrand et al. in preparation).
- Stellar photospheric properties (provided through Legacy deliveries to the Spitzer Science Center; see section 6.3).
- Detected companion properties and limits on undetected companions (e.g. Metchev and Hillenbrand, 2004; 2006).

Selected data tables from these sources are also included in the Spitzer Legacy Science archive (particularly the mid-infrared and sub-millimeter survey data and those data used in fitting photospheric parameters).

6.2. Spitzer Data Products

Spitzer data are provided to the SSC for all 328 stars in the FEPS sample as raw and SSC pipelined products (accessed through LEOPERD) and as “enhanced data products” (<http://ssc.spitzer.caltech.edu/legacy/all.html>).

A Pointed Observations Photometric Catalog (POPC) is available consisting of flux densities for IRAC (3.6, 4.5 and $8.0\mu\text{m}$) and MIPS (24 and $70\mu\text{m}$) observations for all sources. IRAC $5.8\mu\text{m}$ flux densities are available for five stars that were part of the early validation portion of the program. Due to time constraints imposed by slight modifications in the expected SNR based on the updated on-orbit performance of the instruments, we chose to drop the $5.8\mu\text{m}$ band from our general survey rather than decrease the number of targets.² Similarly, $160\mu\text{m}$ observations are available for approximately 10% of the FEPS sample. The confusion limit at $160\mu\text{m}$ for most of our targets was well above the sensitivity level needed to test our toy model for the evolution of our Solar System through observation of sun-like stars from 3 Myr to 3 Gyr. Therefore, we chose a limited campaign of $160\mu\text{m}$ observations in order to preserve the “discovery space” ($> \times 30$ compared to ISO at these wavelengths) enabled by MIPS $160\mu\text{m}$ observations for a random subset of our sample. We also include an image atlas based on mosaicked IRAC and MIPS images. In the case of the MIPS 70 and $160\mu\text{m}$ observations, these images represent the data from which the photometry in the POPC is derived. In the case of the IRAC and MIPS 24 μm data, photometry is derived from individual frames and the results in the POPC are the median values with associated errors as described above.

Low resolution ($R \sim 64\text{--}128$) spectra obtained with the IRS are presented in the spectral atlas comprised of extracted spectra from $7.4 - 33\mu\text{m}$ for all stars and spectra from $5.2 - 33\mu\text{m}$ for 3-30 Myr stars. Again, because of on-orbit sensitivities, we chose to drop the second order of the short low module (providing spectra from $5.2\text{--}7.4\mu\text{m}$) for the older sources in the sample rather than decrease the number of stars in our program. We also plan to deliver an atlas of high resolution ($R \sim 600$) IRS spectra comprised of data from 9.9 to $37.2\mu\text{m}$ for 35 stars chosen from amongst our full sample. Tables of emission line fluxes (or upper limits) are provided for six features selected as most sensitive to remnant gas based on the models of Gorti & Hollenbach (2004).

6.3. Calibration Products

A primary product delivered for all sources in the survey are models of the stellar photosphere fit to short wavelength photometry and extended through the Spitzer wavelengths. The photospheric emission component is modeled by fitting Kurucz atmospheres including convective overshoot to available *BV* Johnson, *vby* Stromgren, *B_TV_T* Tycho, *H_p* Hipparcos, *RI* Cousins, and *JHK_s* 2MASS photometry. Predicted magnitudes were computed as described in Cohen et al. (2003, and references therein) using the combined system response of filter, atmosphere (for ground-based observations), and detector. The best-fit Kurucz model was computed in a least squares sense with the effective temperature and normalization constant (i.e. solid angle of the source physically set by the distance and radius) as free parameters, $[\text{Fe}/\text{H}]$ fixed to solar metallicity, and surface gravity fixed to the value appropriate for the adopted stellar age and mass. Visual extinction is fixed to $A_V = 0^m$ for stars with distances less than 40 pc, assumed to be within the dust-free Local Bubble, but a free parameter for stars at larger distances. A file containing the best-fit stellar spectral energy distribution (SED) is provided along with associated uncertainties in the fitted parameters. These fits are available from the Spitzer Legacy Science Archive (<http://ssc.spitzer.caltech.edu/legacy/all.html>).

Our secondary products include reported information concerning instrument calibration based on observations of FEPS targets that are consistent with the expected level of stellar photospheric emission. We also investigate the consistency between different instruments such as: 1) IRAC photometry at 5.4 and $8.0\mu\text{m}$

²Because FEPS utilized the sub-array mode of IRAC observations reserved for bright stars, we do not obtain $5.8\mu\text{m}$ observations simultaneously with the $3.6\mu\text{m}$ observations as is the usual case.

and the IRS spectra from 5.2–10 μm ; 2) MIPS 24 μm photometry and IRS spectra from 20–26 μm ; and 3) low resolution and high resolution spectra from 9.9–33 μm . Details concerning these diagnostic comparisons can be found in the FEPS Explanatory Supplements that accompany our data releases to the Spitzer Science Center.

7. Summary of Results to Date

We briefly summarize the results from the FEPS program to date. Silverstone et al. (2006) report a search for warm dust excesses surrounding 74 sun-like stars with ages 3–30 Myr. Only five objects show evidence for excess emission between 3.6–8 μm . All appear to be optically-thick disks and four shown signs of active accretion from the disk onto the star. This result suggests that the transition time between optically-thick to optically-thin inside of 1 AU is very short (< 1 Myr). Bouwman et al. (submitted) analyze the dust size and composition in the optically-thick accretion disks in the FEPS sample from IRS high resolution observations. They report a correlation between the inferred grain size and slope of the SED tracing disk structure. They also analyze the contribution of crystalline silicate emission to the observed spectra comparing the results to models for the production of crystalline grains in the disk. Hollenbach et al. (2005) report analysis of the IRS high resolution data for HD 105 (30 Myr old) indicating that less than 0.1 $M_{JUPITER}$ of gas persists between 1–40 AU. Extending this work, Pascucci et al. (2006) report similar results for a sample of 15 stars spanning a range of age from 3–100 Myr. It appears that gas-rich disks capable of forming Jupiter-mass planets dissipate in less than 10 Myr. Additional observations planned will address whether gas-rich disks persist beyond 3 Myr.

Hines et al. (2006) report the discovery of an unusual warm debris disk around the 30 Myr old star HD 12039. Assuming the excess is produced from dust dominated by large black-body grains, the emitting area is estimated to be between 4–6 AU from the star, comparable to the location of our own asteroidal debris belt. Stauffer et al. (2005) analyze the frequency of 24 μm excess emission among sun-like stars in the 100 Myr old Pleiades open cluster. They find a small fraction of stars exhibit excess emission attributable to warm dust in the terrestrial planet zone. Future work will assess the fraction of warm dust excess as a function of age throughout the FEPS sample.

Initial discoveries of cool dust debris (Meyer et al. 2004; Kim et al. 2005) around FEPS targets suggest that: 1) there is large dispersion of inferred dust masses in outer debris belts at any one time; 2) there is a general trend of less dust at later times; and 3) most of these systems have large inner holes in their radial dust distributions. Inner holes of order 30 AU in these disks with large dust mass surface density are probably maintained by mutual collisions of grains whose size are diminished down to the blow-out size whence they are removed from the system due to radiation pressure (Dominik and Decin, 2003; Wyatt, 2005), although we cannot rule out the presence of gas giant planets in most systems. In an analysis of a possible correlation between the presence of debris and radial velocity planets, Moro-Martín et al. (submitted) report no correlation in the FEPS database nor in the published surveys of Bryden et al. (2006), as well as the detection of a debris disk surrounding planet host star HD 38529. Future work will focus on the fraction of objects with excess emission, the evolution in the mean dust mass as a function of age, and the presence of extended debris disks around some stars (Hillenbrand et al., in preparation), as well as connections between the presence of debris and metallicity of the central star.

We would like to thank our colleagues at mission control at JPL, the Spitzer Science Center, as well as members of the IRAC, IRS, and MIPS instrument teams for their contributions to this work. This

work is based in part on observations made with the Spitzer Space Telescope, which is operated by the Jet Propulsion Laboratory, California Institute of Technology under NASA contract 1407. FEPS is pleased to acknowledge support through NASA contracts 1224768, 1224634, and 1224566 administered through JPL. MRM is also supported through membership in NASA’s Astrobiology Institute. S.W. was supported by the German Research Foundation (DFG) through the Emmy Noether grant WO 857/2–1. EEM is supported by a Clay Fellowship from the Smithsonian Astrophysical Observatory. The MPIA team is supported through the European Planet Formation Network funded by the EU.

REFERENCES

- Backman, D.E., & Paresce, F. 1993, *Protostars and Planets III*, 1253
- Beckwith, S.V.W., & Sargent, A.I. 1996, *Nature*, 383, 139
- Beichman, C.A., et al. 2005, *ApJ*, 622, 1160
- Benjamin, R.A., et al. 2003, *PASP*, 115, 953
- Bryden, G., et al. 2006, *ApJ*, 636, 1098
- Burns, J. A., Lamy, P. L., & Soter, S. 1979, *Icarus*, 40,
- Carpenter, J. M., Wolf, S., Schreyer, K., Launhardt, R., & Henning, T. 2005, *AJ*, 129, 1049
- Chiang, E. I., & Goldreich, P. 1997, *ApJ*, 490, 368
- Cohen, M., Megeath, S. T., Hammersley, P. L., Martín-Luis, F., & Stauffer, J. 2003, *AJ*, 125, 2645
- de Muizon, M. J. 2005, *Space Science Reviews*, 119, 201
- Dickinson, M., Giavalisco, M., & The Goods Team 2003, *The Mass of Galaxies at Low and High Redshift*, 324
- Dominik, C., & Decin, G. 2003, *ApJ*, 598, 626
- Duquennoy, A., & Mayor, M. 1991, *A&A*, 248, 485
- Evans, N. J., et al. 2003, *PASP*, 115, 965
- Fazio, G. G., et al. 2004, *ApJS*, 154, 10
- Gomes, R., Levison, H. F., Tsiganis, K., & Morbidelli, A. 2005, *Nature*, 435, 466
- Gordon, K. D., et al. 2004, *Proc. SPIE*, 5487, 177
- Gorti, U., & Hollenbach, D. 2004, *ApJ*, 613, 424
- Greaves, J. S., et al. 1998, *ApJ*, 506, L133
- Guillout, P., Sterzik, M. F., Schmitt, J. H. M. M., Motch, C., & Neuhaeuser, R. 1998, *A&A*, 337, 113
- Henry, T. J., Soderblom, D. R., Donahue, R. A., & Baliunas, S. L. 1996, *AJ*, 111, 439
- Higdon, S. J. U., et al. 2004, *PASP*, 116, 975

- Hines, D. C., et al. 2006, *ApJ*, 638, 1070
- Hollenbach, D., et al. 2005, *ApJ*, 631, 1180
- Houck, J. R., et al. 2004, *ApJS*, 154, 18
- Jura, M. 2004, *ApJ*, 603, 729
- Kalas, P., Liu, M. C., & Matthews, B. C. 2004, *Science*, 303, 1990
- Kennicutt, R. C., et al. 2003, *PASP*, 115, 928
- Kim, J. S., et al. 2005, *ApJ*, 632, 659
- Lagrange, A.-M., Backman, D. E., & Artymowicz, P. 2000, *Protostars and Planets IV*, 639
- Lonsdale, C. J., et al. 2003, *PASP*, 115, 897
- Lorenzetti, D. 2005, *Space Science Reviews*, 119, 181
- Mamajek, E. E., Meyer, M. R., & Liebert, J. 2002, *AJ*, 124, 1670
- Mamajek, E. E., Meyer, M. R., Hinz, P. M., Hoffmann, W. F., Cohen, M., & Hora, J. L. 2004, *ApJ*, 612, 496
- Marcy, G., Butler, R. P., Fischer, D., Vogt, S., Wright, J. T., Tinney, C. G., & Jones, H. R. A. 2005, *Progress of Theoretical Physics Supplement*, 158, 24
- Mathieu, R. D., Ghez, A. M., Jensen, E. L. N., & Simon, M. 2000, *Protostars and Planets IV*, 703
- Metchev, S. A., Hillenbrand, L. A., & Meyer, M. R. 2004, *ApJ*, 600, 435
- Metchev, S. A., & Hillenbrand, L. A. 2006, *ApJ*, 651, in press
- Metchev, S. A., & Hillenbrand, L. A. 2004, *ApJ*, 617, 1330
- Meyer, M. R., et al. 2004, *ApJS*, 154, 422
- Meyer, M. R., Backman, D. E., Weinberger, A. J., & Wyatt, M. C. 2007, *Protostars and Planets V*, B. Reipurth, D. Jewitt, and K. Keil (eds.), University of Arizona Press, Tucson, 951 pp., 2007., p.573-588, 573
- Miyake, K., & Nakagawa, Y. 1993, *Icarus*, 106, 20
- Molster, F., & Kemper, C. 2005, *Space Science Reviews*, 119, 3
- Moro-Martín, A., Wolf, S., & Malhotra, R. 2005, *ApJ*, 621, 1079
- Moro-Martín, A., & Malhotra, R. 2002, *AJ*, 124, 2305
- Moro-Martín, A., & Malhotra, R. 2003, *AJ*, 125, 2255
- Moro-Martín, A., & Malhotra, R. 2005, *ApJ*, 633, 1150
- Najita, J., & Williams, J. P. 2005, *ApJ*, 635, 625
- Pascucci, I., et al. 2006, *ApJ*, 651, 1177

- Rieke, G. H., et al. 2004, *ApJS*, 154, 25
- Soderblom, D. R., & King, J. R. 1999, *ASP Conf. Ser.* 185: IAU Colloq. 170: Precise Stellar Radial Velocities, 185, 102
- Strom, R. G., Malhotra, R., Ito, T., Yoshida, F., & Kring, D. A. 2005, *Science*, 309, 1847
- Torra, J., Fernández, D., Figueras, F., & Comerón, F. 2000, *Ap&SS*, 272, 109
- Weinberger, A. J., Becklin, E. E., Schneider, G., Smith, B. A., Lowrance, P. J., Silverstone, M. D., Zuckerman, B., & Terrile, R. J. 1999, *ApJ*, 525, L53
- Werner, M. W., et al. 2004, *ApJS*, 154, 1
- Williams, J. P., Najita, J., Liu, M. C., Bottinelli, S., Carpenter, J. M., Hillenbrand, L. A., Meyer, M. R., & Soderblom, D. R. 2004, *ApJ*, 604, 414
- Wolf, S., & Hillenbrand, L. A. 2003, *ApJ*, 596, 603
- Wood, B. E., Müller, H.-R., Zank, G. P., Linsky, J. L., & Redfield, S. 2005, *ApJ*, 628, L143
- Wood, B. E., Müller, H.-R., Zank, G. P., & Linsky, J. L. 2002, *ApJ*, 574, 412
- Wyatt, M. C. 2005, *A&A*, 433, 1007

Table 1. Field Stars

Name	RA(J2000) (J2000)	DEC(J2000) (J2000)	Spectral Type
HD 224873	00:01:23.66	+39:36:38.12	K0
HD 377 ^a	00:08:25.74	+06:37:00.50	G2V
HD 691	00:11:22.44	+30:26:58.52	K0V
HD 984	00:14:10.25	-07:11:56.92	F7V
HD 6434	01:04:40.15	-39:29:17.61	G2/3V
HD 6963	01:10:41.91	+42:55:54.50	G7V
HD 7661	01:16:24.19	-12:05:49.33	K0V
HIP 6276	01:20:32.27	-11:28:03.74	G0
HD 8941	01:28:24.36	+17:04:45.20	F8IV-V
HD 9472	01:33:19.03	+23:58:32.19	G0
HD 11850	01:56:47.27	+23:03:04.09	G5
HD 12039 ^a	01:57:48.98	-21:54:05.32	G3/5V
HD 13382	02:11:23.15	+21:22:38.39	G5V
HD 13507	02:12:55.00	+40:40:06.00	G5V
HD 13531	02:13:13.35	+40:30:27.34	G7V
HD 13974	02:17:03.23	+34:13:27.32	G0V
HD 18940	03:03:28.65	+23:03:41.19	G0
HD 19019	03:03:50.82	+06:07:59.82	F8
HD 19668 ^a	03:09:42.28	-09:34:46.46	G8/K0V
HD 21411	03:26:11.11	-30:37:04.13	G8V
HD 26990	04:16:16.50	+07:09:34.15	G0(V)
HD 27466	04:19:57.08	-04:26:19.60	G5V
HD 28495	04:33:54.23	+64:37:59.40	G0
HD 29231	04:34:38.49	-35:39:29.06	G8V
HD 31143	04:51:45.71	-35:50:24.97	K0V
HD 31392	04:54:04.21	-35:24:16.28	K0V
HD 32850	05:06:42.21	+14:26:46.42	G9V
HD 37572	05:36:56.86	-47:57:52.87	K0V
HD 37216	05:39:52.33	+52:53:50.83	G5
HD 37962	05:40:51.97	-31:21:03.95	G5V
HD 37006	05:46:11.89	+78:15:22.61	G0
HD 38529	05:46:34.92	+01:10:05.31	G8III/IV
HD 38949	05:48:20.06	-24:27:50.04	G1V
HD 40647	06:06:05.68	+69:28:34.02	G5
HD 43989	06:19:08.05	-03:26:20.39	G0V
HD 44594 ^b	06:20:06.16	-48:44:28.05	G3V
HD 45270	06:22:30.97	-60:13:07.14	G1V

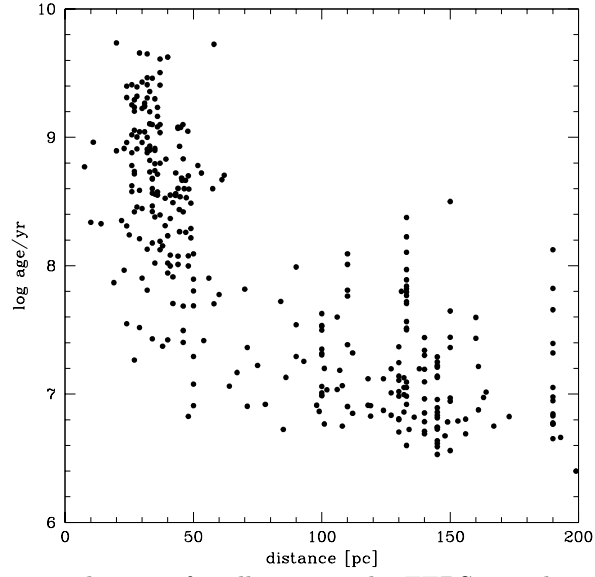


Fig. 3.— Estimated age versus distance for all stars in the FEPS sample, comprised of nearby field stars, open cluster members, and young association members. Typical errors in age are less than 0.5 dex, while typical errors in distance are less than 10 % for stars within 50 parsecs, and within 30 % for more distant targets.

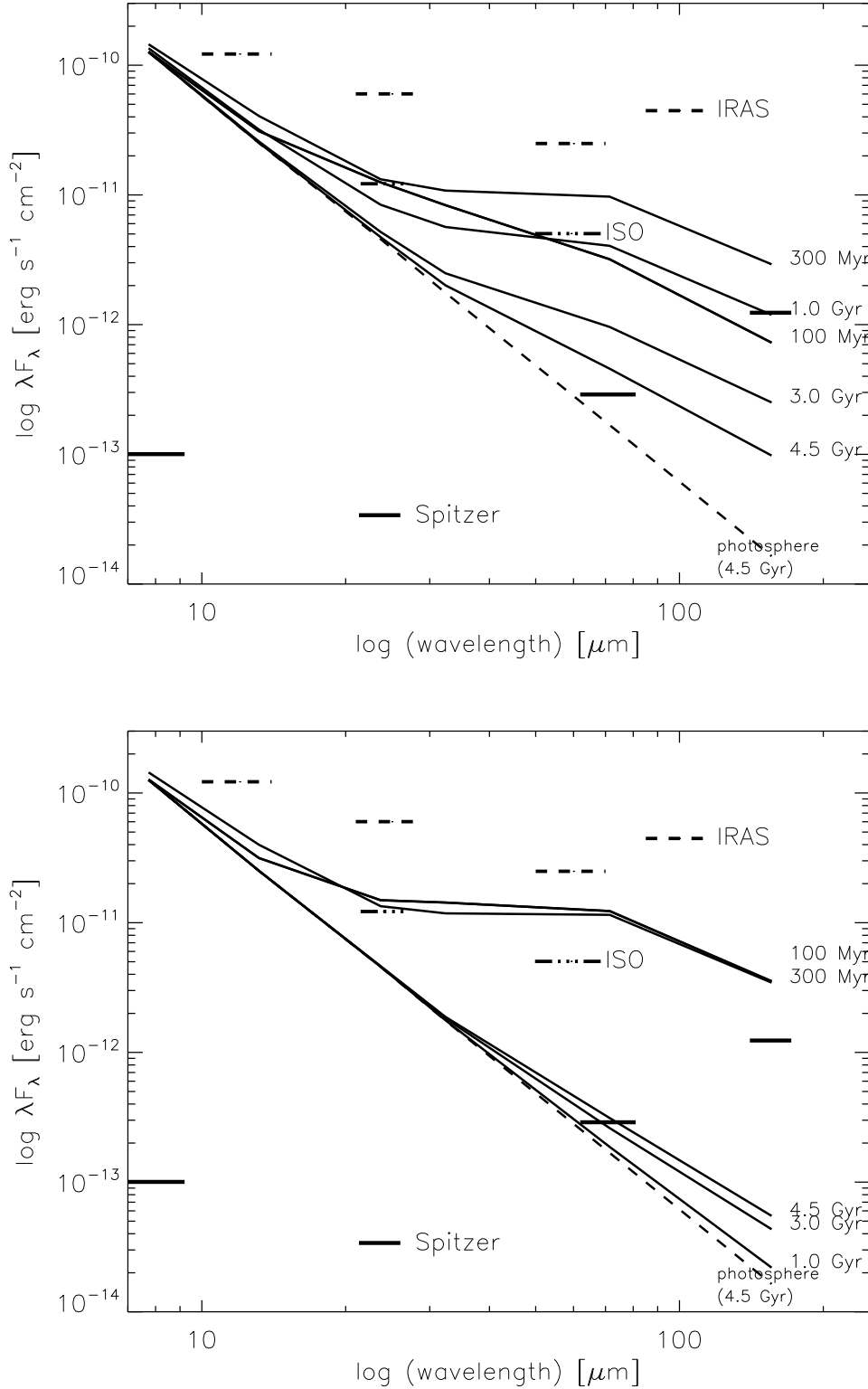


Fig. 4.— Toy model for the evolution of our Solar System debris disk surrounding the Sun as observed from a distance of 30 parsecs. The model shown in the top panel includes continuous removal of planetesimals starting from the minimum mass solar nebula in solids, and evolving towards the present day, without any dramatic clearing event such as the Late Heavy Bombardment. The model shown in the bottom panel begins with the minimum mass solar nebula in solids as in the top panel, but includes a dramatic clearing event such as the Late Heavy Bombardment between 300 Myr and 1 Gyr in accordance with recent models of Gomes et al. (2005; see also Strom et al. 2005).

Table 1—Continued

Name	RA(J2000) (J2000)	DEC(J2000) (J2000)	Spectral Type
HD 61005 ^a	07:35:47.47	-32:12:14.11	G3/5V
HD 60737	07:38:16.44	+47:44:55.34	G0
HD 61994	07:47:30.61	+70:12:23.97	G6V
HD 64324	07:54:48.47	+34:37:11.42	G0
HD 66751	08:10:20.51	+69:43:30.21	F8V
HD 69076	08:15:07.73	-06:55:08.23	K0V
HD 70516	08:24:15.66	+44:56:58.92	G0
HD 71974	08:31:35.05	+34:57:58.44	G5
HD 72687	08:33:15.39	-29:57:23.66	G5V
HD 73668	08:39:43.81	+05:45:51.59	G1V
HIP 42491	08:39:44.69	+05:46:14.00	G5
HD 75302	08:49:12.53	+03:29:05.25	G5V
HD 75393	08:49:15.35	-15:33:53.12	F7V
HD 76218	08:55:55.68	+36:11:46.40	G9-V
HD 77407	09:03:27.08	+37:50:27.72	G0(V)
HD 80606	09:22:37.56	+50:36:13.43	G5
HD 85301	09:52:16.77	+49:11:26.84	G5
HD 88201	10:09:31.78	-32:50:47.95	G0V
HD 88742	10:13:24.72	-33:01:54.22	G0V
HD 90712	10:27:47.79	-34:23:58.14	G2/3V
HD 90905	10:29:42.23	+01:29:27.82	G1V
HD 91782	10:36:47.84	+47:43:12.42	G0
HD 91962	10:37:00.02	-08:50:23.63	G1V
HD 92788	10:42:48.54	-02:11:01.38	G6V
HD 92855	10:44:00.62	+46:12:23.86	F9V
HD 95188	10:59:48.28	+25:17:23.65	G8V
HD 98553	11:20:11.60	-19:34:40.54	G2/3V
HD 100167	11:31:53.92	+41:26:21.65	F8
HD 101472	11:40:36.59	-08:24:20.32	F7V
HD 101959	11:43:56.62	-29:44:51.80	G0V
HD 102071	11:44:39.32	-29:53:05.46	K0V
HD 103432	11:54:32.07	+19:24:40.44	G6V
HD 104576	12:02:39.46	-10:42:49.16	G3V
HD 104860	12:04:33.71	+66:20:11.58	F8
HD 105631	12:09:37.26	+40:15:07.62	G9V
HD 106156	12:12:57.52	+10:02:15.62	G8V
HD 106252	12:13:29.49	+10:02:29.96	G0

Table 1—Continued

Name	RA(J2000) (J2000)	DEC(J2000) (J2000)	Spectral Type
HD 107146	12:19:06.49	+16:32:53.91	G2V
HD 108799	12:30:04.77	-13:23:35.14	G1/2V
HD 108944	12:31:00.74	+31:25:25.84	F9V
HD 112196	12:54:40.02	+22:06:28.65	F8V
HD 115043	13:13:37.01	+56:42:29.82	G1V
HD 121320	13:54:28.20	+20:38:30.46	G5V
HD 121504	13:57:17.23	-56:02:24.27	G2V
HD 122652	14:02:31.63	+31:39:39.09	F8
HD 129333	14:39:00.25	+64:17:29.94	G5V
HD 132173	14:58:30.51	-28:42:34.15	G0V
HD 133295	15:04:33.08	-28:18:00.65	G0/1V
HD 136923	15:22:46.84	+18:55:08.31	G9V
HD 138004	15:27:40.36	+42:52:52.82	G2III
HD 139813	15:29:23.61	+80:27:01.08	G5
HD 141937	15:52:17.55	-18:26:09.80	G2/3V
HD 142229	15:53:20.02	+04:15:11.51	G5V
HD 145229	16:09:26.63	+11:34:28.25	G0
HD 150706	16:31:17.63	+79:47:23.15	G3(V)
HD 150554	16:40:56.45	+21:56:53.24	F8
HD 151798	16:50:05.17	-12:23:14.88	G3V
HD 152555	16:54:08.15	-04:20:24.89	F8/G0V
HD 153458	17:00:01.66	-07:31:53.93	G5V
HD 154417	17:05:16.83	+00:42:09.18	F9V
HD 157664 ^b	17:18:58.47	+68:52:40.61	G0
HD 159222	17:32:00.99	+34:16:15.97	G1V
HD 161897	17:41:06.70	+72:25:13.41	K0
HD 167389	18:13:07.22	+41:28:31.33	F8(V)
HD 170778	18:29:03.94	+43:56:21.54	G5
HD 172649	18:39:42.11	+37:59:35.22	F5
HD 179949	19:15:33.23	-24:10:45.61	F8V
HD 183216	19:29:40.57	-30:47:52.36	G2V
HD 187897	19:52:09.38	+07:27:36.10	G5
HD 190228	20:03:00.77	+28:18:24.46	G5IV
HD 193017	20:18:10.00	-04:43:43.23	F6V
HD 195034	20:28:11.81	+22:07:44.34	G5
HD 199019	20:49:29.30	+71:46:29.29	G5
HD 199598	20:57:39.68	+26:24:18.40	G0V

Table 1—Continued

Name	RA(J2000) (J2000)	DEC(J2000) (J2000)	Spectral Type
HD 200746	21:05:07.95	+07:56:43.59	G5
HD 201219	21:07:56.53	+07:25:58.47	G5
HD 202108	21:12:57.63	+30:48:34.25	G3V
HD 201989	21:14:01.80	-29:39:48.85	G3/5V
HD 203030	21:18:58.22	+26:13:50.05	G8V
HD 204277	21:27:06.61	+16:07:26.85	F8V
HD 205905	21:39:10.14	-27:18:23.59	G2V
HD 206374	21:41:06.19	+26:45:02.25	G6.5V
HD 209393	22:02:05.38	+44:20:35.47	G5
HD 209779	22:06:05.32	-05:21:29.15	G2V
HD 212291	22:23:09.17	+09:27:39.95	G5
HD 216275	22:50:46.34	+52:03:41.21	G0
HD 217343	23:00:19.29	-26:09:13.48	G3V

^aIRS high resolution spectra were also obtained for these stars.

^bThese stars also also Spitzer Space Telescope calibration targets.

Table 2. Open Cluster Stars

Name	RA(J2000)	DEC(J2000)	Spectral Type	Open Cluster
vB 1	03:17:26.39	+07:39:20.90	F8	Hyades
HE 350	03:17:36.93	+48:50:08.50	-	Alpha Per
HE 373	03:18:27.39	+47:21:15.42	-	Alpha Per
HE 389	03:18:50.31	+49:43:52.19	-	Alpha Per
AP 93	03:19:02.76	+48:10:59.61	-	Alpha Per
HE 622	03:24:49.71	+48:52:18.33	-	Alpha Per
HE 696	03:26:19.36	+49:13:32.54	-	Alpha Per
HE 699	03:26:22.22	+49:25:37.52	-	Alpha Per
HE 750	03:27:37.79	+48:59:28.78	F5	Alpha Per
HE 767	03:27:55.02	+49:45:37.16	-	Alpha Per
HE 848	03:29:26.24	+48:12:11.74	F9V	Alpha Per
HE 935	03:31:28.99	+48:59:28.37	F9.5V	Alpha Per
HE 1101	03:35:08.75	+49:44:39.59	-	Alpha Per
HE 1234	03:39:02.91	+51:36:37.11	-	Alpha Per
HII 120	03:43:31.95	+23:40:26.61	-	Pleiades
HII 152	03:43:37.73	+23:32:09.59	G5V	Pleiades
HII 174	03:43:48.33	+25:00:15.83	-	Pleiades
HII 173	03:43:48.41	+25:11:24.19	-	Pleiades
HII 250	03:44:04.24	+24:59:23.40	-	Pleiades
HII 314	03:44:20.09	+24:47:46.16	-	Pleiades
HII 514	03:45:04.01	+25:15:28.23	-	Pleiades
HII 1015	03:46:27.35	+25:08:07.97	-	Pleiades
HII 1101	03:46:38.78	+24:57:34.61	G0V	Pleiades
HII 1182	03:46:47.06	+22:54:52.48	-	Pleiades
HII 1200	03:46:50.54	+23:14:21.06	-	Pleiades
HII 1776	03:48:17.70	+25:02:52.29	-	Pleiades
HII 2147	03:49:06.11	+23:46:52.49	G7IV	Pleiades
HII 2278	03:49:25.70	+24:56:15.43	-	Pleiades
HII 2506	03:49:56.49	+23:13:07.01	-	Pleiades
HII 2644	03:50:20.90	+24:28:00.22	-	Pleiades
HII 2786	03:50:40.08	+23:55:58.94	-	Pleiades
HII 2881	03:50:54.32	+23:50:05.52	K2	Pleiades
HII 3097	03:51:40.44	+24:58:59.41	-	Pleiades
HII 3179	03:51:56.86	+23:54:06.98	-	Pleiades
vB 39	04:22:44.74	+16:47:27.56	G4V	Hyades
vB 49	04:24:12.78	+16:22:44.22	G0V	Hyades
vB 52	04:24:28.33	+16:53:10.32	G2V	Hyades
vB 176	04:25:47.56	+18:01:02.20	K2V	Hyades

Table 2—Continued

Name	RA(J2000)	DEC(J2000)	Spectral Type	Open Cluster
vB 63	04:26:24.61	+16:51:11.84	G1V	Hyades
vB 64	04:26:40.11	+16:44:48.78	G2+	Hyades
vB 66	04:27:46.07	+11:44:11.07	F8	Hyades
vB 73	04:28:48.29	+17:17:07.84	G2V	Hyades
vB 79	04:29:31.61	+17:53:35.46	K0V	Hyades
vB 180	04:29:57.73	+16:40:22.23	K1V	Hyades
vB 88	04:31:29.35	+13:54:12.55	F9V	Hyades
vB 91	04:32:50.12	+16:00:20.96	-	Hyades
vB 92	04:32:59.45	+15:49:08.37	-	Hyades
vB 93	04:33:37.97	+16:45:44.96	-	Hyades
vB 96	04:33:58.54	+15:09:49.04	G5	Hyades
vB 183	04:34:32.18	+15:49:39.23	-	Hyades
vB 97	04:34:35.31	+15:30:16.56	F8:V	Hyades
vB 99	04:36:05.27	+15:41:02.60	-	Hyades
vB 106	04:38:57.31	+14:06:20.16	G5	Hyades
vB 142	04:46:30.38	+15:28:19.38	G5	Hyades
vB 143	04:51:23.22	+15:26:00.45	F8	Hyades
R3	10:29:32.75	-63:49:15.68	-	IC2602
R45	10:40:00.03	-63:15:11.04	-	IC2602
W79	10:42:07.07	-64:46:07.85	-	IC2602
B102	10:42:41.52	-64:21:04.37	-	IC2602
R83	10:46:14.83	-64:02:58.05	-	IC2602

Table 3. Young Stars

Name	RA(J2000)	DEC(J2000)	Spectral Type
HD 105 ^a	00:05:52.56	-41:45:10.98	G0V
QT And	00:41:17.32	+34:25:16.77	G
RE J0137+18A	01:37:39.41	+18:35:33.16	K3Ve
HD 15526	02:29:35.03	-12:24:08.56	G5/6V
1RXS J025216.9+361658	02:52:17.59	+36:16:48.14	K2IV
2RE J0255+474	02:55:43.60	+47:46:47.58	K5Ve
1RXS J025751.8+115759	02:57:51.68	+11:58:05.83	G7V
RX J0258.4+2947	02:58:28.77	+29:47:53.80	K0IV
1RXS J030759.1+302032	03:07:59.20	+30:20:26.05	G5IV
1E 0307.4+1424	03:10:12.55	+14:36:02.90	G6V
1RXS J031644.0+192259	03:16:43.89	+19:23:04.11	G2V
1RXS J031907.4+393418	03:19:07.61	+39:34:10.50	K0V
1E 0324.1-2012	03:26:22.05	-20:01:48.81	G4V
RX J0329.1+0118	03:29:08.06	+01:18:05.66	G0(IV)
RX J0331.1+0713	03:31:08.38	+07:13:24.78	K4(V)/E
HD 22179	03:35:29.91	+31:13:37.45	G5IV
1RXS J034423.3+281224	03:44:24.25	+28:12:23.07	G7V
1RXS J035028.0+163121	03:50:28.40	+16:31:15.19	G5IV
RX J0354.4+0535	03:54:21.31	+05:35:40.77	G2(V)
RX J0357.3+1258	03:57:21.39	+12:58:16.83	G0
HD 25300	03:59:36.73	-39:53:14.85	K0
HD 285281	04:00:31.07	+19:35:20.70	K1
HD 285372	04:03:24.95	+17:24:26.12	K3(V)
HD 284135 ^a	04:05:40.58	+22:48:12.14	G3(V)
HD 281691	04:09:09.74	+29:01:30.55	K1(V)
HD 26182	04:10:04.69	+36:39:12.14	G0V
HD 284266	04:15:22.92	+20:44:16.93	K0(V)
HD 285751	04:23:41.33	+15:37:54.87	K2(V)
HD 279788	04:26:37.40	+38:45:02.37	G5V
HD 285840	04:32:42.43	+18:55:10.25	K1(V)
1RXS J043243.2-152003	04:32:43.51	-15:20:11.39	G4V
RX J0434.3+0226	04:34:19.54	+02:26:26.10	K4e
HD 282346	04:39:31.00	+34:07:44.43	G8V
RX J0442.5+0906	04:42:32.09	+09:06:00.86	G5(V)
HD 31281	04:55:09.62	+18:26:30.84	G1(V)
HD 286179	04:57:00.65	+15:17:53.09	G3(V)
HD 31950	05:00:24.31	+15:05:25.28	-
HD 286264	05:00:49.28	+15:27:00.68	K2IV

Table 3—Continued

Name	RA(J2000)	DEC(J2000)	Spectral Type
1RXS J051111.1+281353	05:11:10.53	+28:13:50.38	K0V
1RXS J053650.0+133756	05:36:50.06	+13:37:56.22	K0V
HD 245567	05:37:18.44	+13:34:52.52	G0V
SAO 150676	05:40:20.74	-19:40:10.85	G2V
AO Men ^a	06:18:28.24	-72:02:41.56	K3.5
HD 47875	06:34:41.04	-69:53:06.35	G3V
RE J0723+20	07:23:43.58	+20:24:58.64	K3(V)
HD 70573	08:22:49.95	+01:51:33.58	G1/2V
RX J0849.2-7735	08:49:11.11	-77:35:58.53	K1(V)
RX J0850.1-7554	08:50:05.41	-75:54:38.11	G5
RX J0853.1-8244	08:53:05.29	-82:43:59.71	K0(V)
RX J0917.2-7744	09:17:10.33	-77:44:01.99	G2
HD 86356	09:51:50.70	-79:01:37.73	G6/K0
SAO 178272	09:59:08.42	-22:39:34.57	K2V
MML 1	10:57:49.37	-69:13:59.99	K1+IV
RX J1111.7-7620 ^a	11:11:46.32	-76:20:09.21	K1
RX J1140.3-8321	11:40:16.59	-83:21:00.38	K2
BPM 87617	11:47:45.73	+12:54:03.31	K5Ve
HD 104467	12:01:39.15	-78:59:16.85	G5III/IV
RX J1203.7-8129	12:03:24.70	-81:29:55.28	K1
HIP 59154	12:07:51.19	-75:55:15.97	K2
RX J1209.8-7344	12:09:42.82	-73:44:41.41	G9
MML 8 ^a	12:12:35.77	-55:20:27.31	K0+IV
MML 9	12:14:34.10	-51:10:12.47	G9IV
HD 106772	12:17:26.94	-80:35:06.90	G2III/IV
RX J1220.6-7539	12:20:34.38	-75:39:28.65	K2
HD 107441	12:21:16.48	-53:17:45.06	G1.5IV
MML 17 ^a	12:22:33.23	-53:33:48.95	G0IV
MML 18	12:23:40.13	-56:16:32.57	K0+IV
RX J1225.3-7857	12:25:13.40	-78:57:34.71	G5
HD 111170	12:47:51.86	-51:26:38.29	G8/K0V
MML 26	12:48:48.19	-56:35:37.90	G5IV
MML 28 ^a	13:01:50.70	-53:04:58.11	K2-IV
MML 32	13:17:56.94	-53:17:56.21	G1IV
HD 116099	13:22:04.47	-45:03:23.19	G0/3
PDS 66 ^a	13:22:07.53	-69:38:12.18	K1IVe
HD 117524	13:31:53.61	-51:13:33.05	G2.5IV
MML 36 ^a	13:37:57.30	-41:34:41.98	K0IV

Table 3—Continued

Name	RA(J2000)	DEC(J2000)	Spectral Type
HD 119269	13:43:28.54	-54:36:43.44	G3/5V
MML 38	13:47:50.55	-49:02:05.61	G8IVe
HD 120812	13:52:47.80	-46:44:09.24	F8/G0V
MML 40	14:02:20.72	-41:44:50.93	G9IV
MML 43	14:27:05.56	-47:14:21.73	G7IV
HD 126670	14:28:09.30	-44:14:17.54	G6/8III/IV
HD 128242	14:37:04.22	-41:45:02.91	G3V
RX J1450.4-3507	14:50:25.82	-35:06:48.66	K1(IV)
MML 51	14:52:41.98	-41:41:55.24	K1IVe
RX J1457.3-3613	14:57:19.62	-36:12:27.44	G6IV
RX J1458.6-3541	14:58:37.69	-35:40:30.27	K3(IV)
RX J1500.8-4331	15:00:51.89	-43:31:21.23	K1(IV)
MML 57	15:01:58.82	-47:55:46.46	G1.5IV
RX J1507.2-3505	15:07:14.81	-35:04:59.55	K0
HD 135363	15:07:56.31	+76:12:02.66	G5(V)
HD 133938	15:08:38.50	-44:00:51.99	G6/8III/IV
RX J1518.4-3738	15:18:26.92	-37:38:02.14	K1
RX J1531.3-3329	15:31:21.93	-33:29:39.46	K0
HIP 76477	15:37:11.30	-40:15:56.70	G9
V343 Nor ^a	15:38:57.57	-57:42:27.30	K0V
HD 139498	15:39:24.40	-27:10:21.87	G8(V)
RX J1541.1-2656	15:41:06.79	-26:56:26.33	G7
RX J1544.0-3311	15:44:03.76	-33:11:11.09	K1
HD 140374	15:44:21.06	-33:18:54.97	G8V
RX J1545.9-4222	15:45:52.25	-42:22:16.41	K1
HD 141521	15:51:13.74	-42:18:51.36	G8V
HD 141943 ^a	15:53:27.29	-42:16:00.81	G0/2V
HD 142361 ^a	15:54:59.86	-23:47:18.26	G3V
[PZ99] J155847.8-175800	15:58:47.73	-17:57:59.58	K3
RX J1600.6-2159 ^a	16:00:40.57	-22:00:32.24	G9
HD 143358	16:01:07.93	-32:54:52.65	G1/2V
ScoPMS 21	16:01:25.63	-22:40:40.38	K1IV
ScoPMS 27	16:04:47.76	-19:30:23.12	K2IV
[PZ99] J160814.7-190833	16:08:14.74	-19:08:32.77	K2
ScoPMS 52 ^a	16:12:40.51	-18:59:28.31	K0IV
[PZ99] J161318.6-221248	16:13:18.59	-22:12:48.96	G9
[PZ99] J161329.3-231106	16:13:29.29	-23:11:07.56	K1
[PZ99] J161402.1-230101	16:14:02.12	-23:01:02.18	G4

Table 3—Continued

Name	RA(J2000)	DEC(J2000)	Spectral Type
[PZ99] J161411.0-230536 ^a	16:14:11.08	-23:05:36.26	K0
[PZ99] J161459.2-275023 ^a	16:14:59.18	-27:50:23.06	G5
[PZ99] J161618.0-233947	16:16:17.95	-23:39:47.70	G7
HD 146516	16:17:31.39	-23:03:36.02	G0IV
ScoPMS 214 ^a	16:29:48.70	-21:52:11.91	K0IV
RX J1839.0-3726	18:39:05.29	-37:26:21.78	K1
RX J1841.8-3525	18:41:48.56	-35:25:43.71	G7
RX J1842.9-3532 ^a	18:42:57.98	-35:32:42.73	K2
RX J1844.3-3541	18:44:21.92	-35:41:43.53	K5
RX J1852.3-3700 ^a	18:52:17.30	-37:00:11.93	K3
HD 174656	18:53:05.99	-36:10:22.91	G6IV
RX J1917.4-3756 ^a	19:17:23.83	-37:56:50.52	K2
HD 199143	20:55:47.68	-17:06:51.02	F8V
V383 Lac	22:20:07.03	+49:30:11.67	K0IV/V
RX J2313.0+2345	23:13:01.24	+23:45:29.64	F8
HD 219498	23:16:05.02	+22:10:34.98	G5

^aIRS high resolution spectra were also obtained for these stars.

Table 4. Pre-selected IRS High Resolution Targets

Name	RA(J2000)	DEC(J2000)	Spectral Type
HD 8907	01:28:34.35	+42:16:03.70	F8
HD 17925	02:52:32.14	-12:46:11.18	K1V
HD 25457	04:02:36.76	-00:16:08.17	F7V
HD 35850	05:27:04.77	-11:54:03.38	F7/8V
HD 37484	05:37:39.63	-28:37:34.65	F3V
HD 38207 ^a	05:43:20.95	-20:11:21.41	F2V
HD 41700	06:04:28.44	-45:02:11.71	F8/G0V
HD 72905 ^a	08:39:11.62	+65:01:15.14	G1.5VB
HD 134319	15:05:49.90	+64:02:50.00	G5(V)
HD 143006	15:58:36.92	-22:57:15.35	G6/8
HD 191089 ^a	20:09:05.22	-26:13:26.63	F5V
HD 202917	21:20:49.95	-53:02:03.05	G5V
HD 209253	22:02:32.97	-32:08:01.60	F6/7V
HD 216803	22:56:24.07	-31:33:56.12	K4VP

^aIRS high resolution spectra were not obtained for these sources due to program constraints.